ARTICLE

Title:

Assay to visualize specific protein oxidation reveals spatio-temporal regulation of SHP2

Authors:
Ryouhei Tsutsumi[1,*], Jana Harizanova[2], Rabea Stockert[2], Katrin Schröder[3], Philippe I. H. Bastiaens[2,4], and Benjamin G. Neel[1]

Affiliation:
[1]Perlmutter Cancer Center, New York University Langone Medical Center, 430 East 29th Str., New York, NY10016, USA.
[2]Department of Systemic Cell Biology, Max Planck Institute of Molecular Physiology, Otto-Hahn-Str. 11, 44227 Dortmund, Germany.
[3]Institute of Physiology, Goethe-University, Theodor-Stern-Kai 7, 60590 Frankfurt, Germany.
[4]Faculty of Chemistry and Chemical Biology, Technical University of Dortmund, Otto-Hahn Str. 11, 44227 Dortmund, Germany.

*Correspondence should be addressed to R.T. (e-mail: Ryohei.Tsutsumi@nyumc.org)

Abstract

Reactive oxygen species (ROS) are produced transiently in response to cell stimuli, and function as second messengers that oxidize target proteins. Protein-tyrosine phosphatases (PTPs) are important ROS targets, whose oxidation results in rapid, reversible, catalytic inactivation. Despite increasing evidence for the importance of PTP oxidation in signal transduction, the cell biological details of ROS-catalyzed PTP inactivation have remained largely unclear, due to our inability to visualize PTP oxidation in cells. By combining proximity ligation assay (PLA) with chemical labeling of cysteine residues in the sulfenic acid state, we visualize oxidized Src homology 2 domain-containing protein-tyrosine phosphatase 2 (SHP2). We find that platelet-derived growth factor (PDGF) evokes transient oxidation on or close to RAB5+/EEA1- endosomes. SHP2 oxidation requires NADPH oxidases (NOXs), and oxidized SHP2 co-localizes with PDGF receptor and NOX1/4. Our data demonstrate spatially and temporally limited protein oxidation within cells, and suggest that PDGF-dependent "redoxosomes," contribute to proper signal transduction.

Introduction

Multiple studies suggest that ROS (e.g., superoxide ($O_2^{\cdot -}$), hydrogen peroxide (H_2O_2), nitric oxide (NO)) are not merely toxic byproducts of cellular metabolism, but also function as second messengers that regulate specific signaling molecules[1]. Various stimuli, including cytokines and growth factors, such as interleukin-1 (IL-1), tumor necrosis factor α (TNFα) and PDGF, transiently evoke ROS production, and receptor-evoked ROS are required for precise regulation of at least some signal transduction events[1]. ROS can damage cellular macromolecules, suggesting that signal transduction-associated ROS must be regulated in a spatio-temporal manner. Several reports argue that production of ROS in response to IL-1 or TNFα occurs in a specialized endosomal compartment, which has been termed the "redoxosome"[2]. Whether redoxosomes contribute to other types of signaling pathways (e.g., by classical growth factors) has remained unclear, and the identity of specific proteins oxidized by redoxosomes has remained elusive.

Protein-tyrosine phosphatases (PTPs) regulate intracellular signal transduction by receptor tyrosine kinases (RTKs), cytokine receptors and integrins[3]. All PTPs share a conserved active site "signature motif," -[I/V]HCSXGXGR[S/T]G-, featuring an unusually acidic catalytic cysteinyl (Cys) residue that executes a nucleophilic attack on substrate phosphotyrosyl (p-Tyr) residues[4]. The same properties that confer a low pK_a on the catalytic cysteine also render it highly susceptible to oxidation[3-5]. Consequently, PTPs have emerged as important ROS targets, which undergo transient oxidation and inactivation

downstream of various upstream stimuli[5-7].

In response to physiological levels of ROS, PTP catalytic Cys residues are oxidized to the sulfenic acid state (SOH). Depending upon the specific enzyme, this Cys-SOH rapidly reacts with the adjacent main chain amido-nitrogen to form an intramolecular sulfenylamide (S-N) bond[7,8], or with a vicinal cysteinyl residue to form an intra- or intermolecular disulfide (S-S) bond[7]. These oxidized states of PTPs are reversible, and can be reduced by the glutathione (GSH) or thioredoxin systems. Higher levels of ROS result in biologically irreversible PTP oxidation to the sulfinic, sulfonic or sulfone states[7]. ROS-dependent, reversible inactivation of PTPs is believed to help fine tune phosphotyrosine-based signal transduction[1,6,7]. Support for this concept has been obtained mainly by biochemical approaches[9-12], as technical limitations have, in general, precluded investigation of the spatio-temporal nature of PTP oxidation.

SHP2, encoded by *PTPN11*, is required for normal RAS/mitogen-activated protein kinase (MAPK) activation by multiple growth factors, including PDGF, epidermal growth factor (EGF), and many others[13,14]. SHP2 reportedly is oxidized in response to multiple cellular stimuli, including PDGF[15,16], but the spatio-temporal dynamics, regulatory mechanism, physiological role and source of ROS for SHP2 oxidation have not been defined.

Here, we report an easy, sensitive, and potentially general method that specifically visualizes oxidized proteins. Focusing mainly on PDGF signaling, we find

that SHP2 oxidation in response to cell stimulation is regulated spatially and temporally. Combining our approach with "nearest neighbor" object-based image analysis, we show that SHP2 oxidation occurs at, or in close proximity to, RAB5+/early endosome antigen 1 (EEA1)- endosomes, and requires specific cellular NOX proteins. Our results implicate "redoxosomes" in PDGF-dependent ROS production and signaling. Our assay also can visualize oxidation of another PTP, protein-tyrosine phosphatase 1B (PTP1B) in response to insulin.

Results

Visualization of oxidized SHP2 by dimedone-PLA

Dimedone is a cell-permeable, soft nucleophile that reportedly labels cysteine-sulfenic acids state, but not cysteines in the thiol, disulfide, sulfinic or sulfonic acid state[17,18]. To evaluate the applicability of these observations to PTPs, we assessed the specificity in *in vitro* labeling experiments using PTP1B, the oxidation profile of which was established previously[8]. As monitored by *in vitro* phosphatase activity, purified recombinant PTP1B sequentially underwent reversible, followed by irreversible, oxidation, in response to increasing concentrations of H_2O_2[8] (Supplementary Fig. 1a). Also, as expected[19], PTP1B was oxidized irreversibly by treatment with pervanadate (Supplementary Fig. 1a). We then labelled PTP1B with dimedone (5 mM) in the presence of dithiothreitol (DTT), H_2O_2, or pervanadate, and detected dimedone-labeled PTP1B by immunoblotting with an antiserum that specifically recognizes dimedonylated cysteinyl residues[20]. Dimedone labelled PTP1B best at low H_2O_2 concentrations, but did not react with PTP1B in the presence of pervanadate (Supplementary Fig. 1b). These data support the previous conclusion that dimedone reacts only with reversibly oxidized thiols[18]. Notably, pre-incubating purified PTP1B in 80 μM H_2O_2 (which favors reversible oxidation) before labeling diminished the efficiency of dimedonylation, compared with simultaneous oxidation and dimedone-labeling (Supplementary Fig. 1c). Previous reports have shown that, upon initial oxidation, the cysteine-sulfenic acid of PTP1B (PTP1B-SOH) is converted

to an intramolecular sulfenylamide bond (PTP1B-SN) in PTP1B crystals[8] and in cells[21]. Taken together with these results, our biochemical data suggest that dimedone preferentially labels reversibly oxidized PTP1B in the PTP1B-SOH state, and labels the PTP1B-SN form poorly if at all (see Discussion).

We used anti-dimedone-Cys antiserum to immunostain oxidized proteins in Swiss 3T3 mouse fibroblasts. Fibroblasts were exposed to PDGF (50 ng ml^{-1}), H_2O_2 (1 mM) or left untreated, and then labeled with dimedone (5 mM) for 5 min while undergoing paraformaldehyde-fixation. Fixed, dimedone-labeled cells were then immunostained with anti-dimedone-Cys antiserum. Consistent with an earlier report[20], dimedone-labeled proteins were detected throughout cells, and total fluorescence intensity was increased slightly by H_2O_2 treatment (Supplementary Fig. 1d). By contrast, PDGF-stimulation did not cause a detectable change in the total intensity of anti-dimedone-Cys immunolabeling, most likely reflecting a low amount of oxidized proteins in response to growth factor compared with H_2O_2 (Supplementary Fig. 1d). Treatment of cells with excess H_2O_2 (50 mM) diminished anti-dimedone-Cys antibody labeling, again supporting the selectivity of dimedone for reversibly oxidized proteins (Supplementary Fig. 1e). Of note, anti-dimedone-Cys immunoblots of lysates from dimedone-labeled Swiss 3T3 cells (Supplementary Fig. 1f) revealed that SHP2 is not a major dimedone-labeled protein in these cells. Likewise, there was no appreciable change in overall fluorescence signal when immortalized mouse embryo fibroblasts (MEFs) with or without SHP2[22] were labeled

with dimedone and immunostained with anti-dimedone-Cys antibodies (Supplementary Fig. 1g).

Therefore, we attempted to "optically purify" the oxidized SHP2 (ox-SHP2) signal from the large population of oxidized (and subsequently, dimedonylated) proteins in cells. To do so, we combined dimedone-labeling/anti-dimedone-Cys antibody binding with anti-SHP2 antibody binding, followed by PLA[23] (hereafter, dimedone-PLA). PLA detects any two antibodies that co-localize within ~40 nm[23], in our method, anti-dimedone-Cys and anti-SHP2 antibodies, respectively (Fig. 1a). Dimedone-PLA for SHP2 visualized ox-SHP2 as puncta; notably, the number of puncta increased markedly in cells stimulated with PDGF-BB (50 ng ml^{-1}), EGF (50 ng ml^{-1}), or H_2O_2 (1 mM) for 10 min (Fig. 1b and Supplementary Fig. 2a). Dimedone-PLA puncta were observed mainly in the cytoplasm (Fig. 1b), even though SHP2 is found both in the cytoplasm and the nucleus[24].

Several lines of evidence indicate that these puncta represent ox-SHP2. First, the signals were eliminated in cells that did not undergo dimedone-labeling or that were incubated without anti-dimedone-Cys or anti-SHP2 antibodies (Supplementary Fig. 2b). Likewise, almost no puncta were observed in *Ptpn11*$^{-/-}$ MEFs, generated by Cre recombinase-mediated excision of a conditional (floxed) *Ptpn11* allele[22] (Fig. 1c). Re-expression of wild type (WT) SHP2, but not SHP2 bearing a C459E mutation ($SHP2^{C459E}$) that alters the cysteinyl residue in the SHP2 "signature motif," restored ROS-dependent puncta to *Ptpn11*$^{-/-}$ MEFs (Supplementary Fig. 2c,d). Depleting cellular

ROS with *N*-acetyl-*L*-cysteine (NAC) suppressed dimedone-PLA signals. Conversely, lowering glutathione levels by treatment with the glutathione synthesis inhibitor *L*-buthionine-*S*,*R*-sulfoximine (BSO), enhanced the PLA signal (Supplementary Fig. 2e).

Dimedone-PLA also detects PTP1B oxidation

In principle, our method should be applicable to any reversibly oxidized protein, as long as its oxidation proceeds through a sulfenic acid state and there is specific antibody for the protein that can be used for PLA. Indeed, we detected oxidized PTP1B (ox-PTP1B) in H_2O_2-treated Swiss 3T3 fibroblasts by dimedone-PLA (Supplementary Fig. 3a). Notably, PDGF did not increase the number of puncta for ox-PTP1B. Previous studies have shown that PTP1B oxidation is evoked by insulin stimulation[21,25]. As Swiss 3T3 fibroblasts respond weakly to insulin, we tested HepG2 cells (Supplementary Fig. 3b). HepG2 cells expressing shRNA against endogenous *PTPN1*, which encodes PTP1B, were infected with a lentivirus harboring either WT mouse PTP1B (mPTP1B) or a serine substitution mutant of the catalytic cysteine residue (mPTP1B^{C215S}) (Supplementary Fig. 3c,d). As expected, insulin stimulation evoked a significant increase in dimedone-PLA signal in WT mPTP1B-expressing HepG2 cells, but not in cells expressing mPTP1B^{C215S} (Fig. 2). These results indicate that our method is not restricted to ox-SHP2 detection, but is applicable to other PTPs, and likely non-PTPs as well.

Localization of PDGF-evoked SHP2 oxidation

Upon stimulation with appropriate growth factors, RTKs, including the PDGF receptor (PDGFR), are activated, trans-phosphorylated, and recruit multiple signal relay proteins containing SH2 or phosphotyrosine binding (PTB) domains, including SHP2[26,27]. Activated RTKs are endocytosed into clathrin-coated vesicles, clathrin dissociates, and transport occurs sequentially into early endosomes, late endosomes, and finally to lysosomes to be degraded. Some endocytosed RTKs can be recycled back to the plasma membrane[27,28].

We asked when and where SHP2 oxidation occurs during this sequence. Stimulation of Swiss 3T3 cells with PDGF or EGF (50 ng ml^{-1} each) led to a transient increase of ox-SHP2 to 2-3 fold over basal levels. Ox-SHP2 levels peaked at 5-10 min, and then decreased to ~1.5-fold basal levels by 60-120 min (Fig. 3a and Supplementary Fig. 4a). These findings are consistent with previous biochemical studies that reported SHP2 oxidation in response to PDGF stimulation[15], although EGF-induced SHP2 oxidation has not been reported heretofore. Surface PDGFRβ was endocytosed rapidly, with decreased surface immunofluorescence detectable within 2.5 min after PDGF stimulation (Supplementary Fig. 4b). Hence, maximal SHP2 oxidation occurs at an early stage of PDGFR trafficking.

We next analyzed the dynamics of PDGF-induced SHP2 oxidation in space and time by co-staining dimedone-PLA-labeled cells with antibodies against PDGFRβ, clathrin

heavy chain (CHC), and the early endosome markers RAB5 and EEA1 at various times after PDGF addition. PDGFR, CHC and RAB5 fluorescence also localized to puncta, which overlapped with ox-SHP2 signals at different times after stimulation (Fig. 3b left). PLA generates relatively sparse, large and pleomorphic puncta, reflecting the extended DNA strands that amplify the fluorescence signals. Typical co-localization metrics, such as Pearson's or Manders' coefficients, are not appropriate for assessing co-localization between PLA signals and immunostained intracellular structures, as these coefficients assume that the intensity in each pixel represents a large number of molecules (also see Methods). To determine whether the ox-SHP2 signals were randomly (i.e., stochastically) distributed within cells, or rather were in association/proximity with specific intracellular compartments, we developed an object-based image analysis. The punctate signals for ox-SHP2 and each marker were segmented, the center of mass for each puncta was determined, and the distance of each ox-SHP2 signal to the nearest marker signal was quantified. Notably, the median distance from the ox-SHP2 puncta to the PDGFRβ or CHC signals showed a transient decrease at 2.5 min after PDGF stimulation to ~0.30 μm or ~0.40 μm, respectively, whereas the distance from ox-SHP2 to RAB5 remained at ~0.30 μm over the entire 120 min observation period (Fig. 3b right). The median radius of the ox-SHP2 puncta themselves was ~0.55 μm, which is larger than the distance between ox-SHP2 and the PDGFRβ, CHC and RAB5, respectively. Furthermore, the distance between PDGFRβ, CHC and RAB5 signals, respectively, was larger than the distance

between ox-SHP2 and each of these molecules (Supplementary Fig. 4c). By contrast, the median distance between ox-SHP2 and the nearest EEA1 signal was ~0.85 μm over the entire observation period, which was comparable to the median distance between each EEA1 punctum (Fig. 3b and Supplementary Fig. 4c). These data indicate that ox-SHP2 is transiently in close proximity to PDGFRβ and CHC at early times after PDGF stimulation, RAB5 and ox-SHP2 are constitutively in proximity, and ox-SHP2 does not co-localize with EEA1. Semi-super resolution microscopy (AiryScan) confirmed the adjacency of ox-SHP2 puncta with RAB5+, but not with EEA1+, vesicles (Fig. 3c). Consistent with these observations, ox-SHP2 did not co-localize with the late endosomal markers RAB7 and RAB9 or with the recycling endosomal marker RAB11[29] (Supplementary Fig. 4d). PLA signals generated by anti-extracellular signal–regulated kinase 2 (ERK2) and anti-phospho ERK antibodies were distributed throughout the cytoplasm and nucleus, but showed no specific co-localization with RAB5 (Supplementary Fig. 4e). These results argue against artifactual co-localization of RAB5 with any punctate signal and for the specificity of ox-SHP2/RAB5 co-localization.

RAB5+ endocytic vesicles recruit EEA1 for tethering and fusion to early endosomes[29,30]. Therefore, our results suggest that SHP2 binds to, and is endocytosed with, PDGFRβ (or rapidly associates with the receptor at the clathrin-coated vesicle stage), and undergoes oxidation during the clathrin coated-vesicle/early phase of the endocytic process before reaching EEA1+ early endosomes. Consistent with this model,

immunostaining reveals the presence of a pool of RAB5+/EEA1- vesicles (Supplementary Fig. 4f). By contrast, ox-SHP2 signals do not colocalize with RAB5 in H_2O_2-treated cells (Supplementary Fig. 4g). Hence, H_2O_2-evoked SHP2 oxidation, unlike growth factor induced oxidation, does not proceed through an endosomal compartment and presumably can occur randomly in the cytoplasm. Failure of ox-SHP2 to co-localize with EEA1 at any time (Fig. 3b,c) presumably reflects reduction/re-activation of PDGFR-bound SHP2 at EEA1+ early endosomes or dissociation of ox-SHP2 from PDGFR.

To ask if growth factor-dependent receptor endocytosis is necessary for SHP2 oxidation, we assessed the effects of the dynamin inhibitor Dynasore[31] and the clathrin inhibitor Pitstop® 2[32]. Treatment of Swiss 3T3 cells with either inhibitor abolished the PDGF-dependent increase of ox-SHP2 without affecting H_2O_2-evoked ox-SHP2 generation (Supplementary Fig. 5a). Expression of dynamin2^{K44A}, which acts as a dominant negative mutant[33], also suppressed PDGF-dependent SHP2 oxidation (Fig. 3d and Supplementary Fig. 5b). Collectively, these data establish that clathrin/dynamin-dependent endocytosis is necessary for PDGF-dependent SHP2 oxidation. However, inhibiting endocytosis (either pharmacologically or with dominant negative dynamin2) also decreased overall PDGFRβ tyrosyl phosphorylation (Supplementary Fig. 5c,d). Therefore, it is unclear whether endocytosis is required to trigger SHP2 oxidation *per se* or merely is necessary for maximum PDGFR activation, and ultimately, PDGF-evoked ROS production.

NOX complexes are necessary for PDGF-evoked SHP2 oxidation

Since the first report of PDGF-induced ROS production by Finkel and co-workers[34], the source, location and pathway mediating ROS generation have remained unclear/controversial. One proposed mechanism involves growth factor-evoked activation of non-phagocytic NOX complexes, possibly via phosphoinositide 3-kinase (PI3K) and the small G protein RAC1[35,36]. Other studies implicate mitochondria as the source of growth factor-evoked ROS, via a pathway involving p66SHC (Src homologous and collagen)[37]. NOX family members and the mitochondrial Complexes I/III produce $O_2{\cdot}^-$, which is dismutated to H_2O_2 by superoxide dismutases (SODs)[1]. Catalase specifically decomposes H_2O_2, and exogenous expression of a catalase mutant that localizes to the cytoplasm blocked PDGF-evoked SHP2 oxidation (Fig. 4a and Supplementary Fig. 6a). Hence, H_2O_2 is responsible for PDGF-dependent SHP2 oxidation. Furthermore, the NOX inhibitor diphenyleneiodonium (DPI) or the more selective inhibitor imipramine-blue[38] significantly suppressed PDGF-, but not H_2O_2-evoked SHP2 oxidation (Fig. 4b). By contrast, the mitochondria-targeted anti-oxidant MitoQ[39] had no apparent effect on PDGF-induced ox-SHP2 levels (Supplementary Fig. 6b). These results implicate NOX complex(es), rather than the mitochondrial electron transport chain, as the main source of ROS for PDGF-induced SHP2 oxidation. Consistent with a report implicating PI3K in PDGF-evoked ROS production[36], the PI3K inhibitors LY294002 or BKM120 antagonized PDGF-evoked ox-SHP2 generation (Supplementary Fig. 6c,d).

In mice, the NOX family comprises six transmembrane heme-containing proteins (NOX1-4 and DUOX1,2)[40]. Each NOX or DUOX forms a complex with other subunits (e.g., p22phox or DUOXA1/2) that regulate NOX activity. The topology of NOX/DUOX complexes predicts that if activation were to occur at the plasma membrane, then reduction of NADPH to $NADP^+$ on the cytoplasmic side of membranes would be coupled to extracellular $O_2{\cdot}^-$ production. $O_2{\cdot}^-$ could move to the cytosol through a specific transporter or dismutate to H_2O_2, and then access the cytosol via channels or by diffusion[40], although such a process would seem to be inefficient.

To evaluate the involvement of specific NOXs in PDGF-evoked SHP2 oxidation, we used primary mouse dermal fibroblasts (MDFs) from wild type (WT-MDF) or *Nox1*, *Nox2*, and *Nox4* triple-knockout animals (TKO-MDF) (ref. 41 and Supplementary Fig. 7a,b). Consistent with our inhibitor experiments, PDGF-, but not H_2O_2-evoked SHP2 oxidation was abrogated in TKO-MDFs compared with their WT counterparts (Fig. 4c). Hence, PDGF-induced SHP2 oxidation requires NOX1, NOX2 and/or NOX4.

Ox-SHP2 localizes with endosomes containing NOX proteins

To obtain insight into which NOX complex(es) is/are involved in PDGF-dependent SHP2 oxidation, we co-stained ox-SHP2 with antibodies for each of the NOXs or p22phox. NOX proteins and p22phox showed punctate staining, some of which overlapped with ox-SHP2 PLA puncta (Fig. 4d top). Using object-based image analysis, we found that

PDGF-evoked ox-SHP2 signals were closely associated with NOX1 (median distance ~0.26 μm), NOX4 (median distance ~0.27 μm) and p22phox (median distance ~0.26 μm), but not with NOX2 or NOX3 (median distances ~0.65 μm and ~ 0.87 μm, respectively) (Fig. 4d bottom). Again, the median distances of ox-SHP2 puncta to NOX1, NOX4, or p22phox puncta were significantly less than those between NOX puncta themselves (Supplementary Fig. 7c). Proximity of ox-SHP2 to NOX1, NOX4 and p22phox was observed before and after PDGF stimulation (Supplementary Fig. 7c), and semi-super resolution microscopy confirmed the adjacency of ox-SHP2 to NOX1 and NOX4 (Supplementary Fig. 7d). NOX1 and NOX4 were not visualized at the plasma membrane, mitochondria or in EEA1+ vesicles, although we cannot exclude the possibility that a small fraction of these proteins are found in these structures. Nevertheless, immunostaining revealed NOX1/4 localization to vesicular-like structures that partially co-localized with the ER marker calnexin (Supplementary Fig. 7e). The specificity of each of these antibodies for their respective NOX protein was confirmed by comparing staining of WT- and TKO-MDFs (Supplementary Fig. 7b).

Taken together, our data implicate NOX1 and/or NOX4 in PDGF-evoked SHP2 oxidation. Because our experiments also show that SHP2 oxidation occurs on, or close to, RAB5+ endosomes (see Fig. 3b,c), the overlap of ox-SHP2, NOX1 and/or NOX4 signals presumably occurs on, or close to, such vesicles, which also contain ligand-bound, endocytosed PDGFR. EGF-evoked SHP2 oxidation also occurred in close proximity to

RAB5 and NOX1/4 (Supplementary Fig. 7f). These findings argue that SHP2 oxidation occurs on, or close to, endosomal structures marked by RAB5, but not EEA1, that promote localized ROS generation, consistent with "redoxosomes[2]". Although our object-based analysis has insufficient resolution to determine whether SHP2 oxidation actually occurs on (versus close to) these structures, we note that earlier biochemical studies indicated that SHP2 oxidation was strictly associated with the PDGFR (which, in turn, would be on endocytosed vesicles)[15].

PDGF-evoked redoxosome formation

The "redoxosome" model proposes that IL-1 or TNFα generates NOX-containing, redox-active endosomes wherein ROS generation is directed into membrane-enclosed vesicles (as a consequence of NOX topology)[2]. Our data suggest that PDGF stimulation also promotes redoxosome generation; i.e., NOX1 and/or NOX4 are recruited following PDGFR endocytosis, contribute to ROS production at RAB5+ endosomes, and result in oxidation of SHP2 (and possibly other targets). Indeed, NOX1 and NOX4 showed partial, but significant co-localization with RAB5 (Supplementary Fig. 8a). When calculated by Manders' coefficient, RAB5 co-localization with NOX1/NOX4 decreased slightly upon PDGF stimulation, although substantial co-localization remained (Supplementary Fig. 8a). On the other hand, NOX4 and p22phox, and to a lesser extent, NOX1, showed strongly increased co-localization with PDGFRβ at 5 min after PDGF stimulation (Fig. 5a),

indicating recruitment of NOX proteins to PDGFR-containing vesicles.

To localize PDGF-evoked ROS generation, we utilized the sensor HyPer3[42], targeted selectively to different intracellular locales. HyPer3 is a circularly permuted yellow fluorescent protein (cpYFP) integrated into the regulatory domain of the H_2O_2-sensing protein OxyR, which exhibits increased fluorescence intensity in response to increased local concentrations of H_2O_2[42]. Time-lapse imaging of Swiss 3T3 fibroblasts showed that the fluorescence intensity of HyPer3 fused to the KRAS C-terminal sequence (HyPer3-tk), which is targeted to the plasma membrane, as well as that of HyPer3 fused to RAB5 (HyPer3-RAB5) such that the sensor faces the cytosol on RAB5+ vesicles, increased within 3-6 min of PDGF stimulation (Fig. 5b). By contrast, there was no detectable increase in the fluorescence of cytoplasmic HyPer3 (HyPer3-cyto) or HyPer3 fused with RAB7 (HyPer3-RAB7) in response to PDGF (Fig. 5b). Notably, EGFP, which is not sensitive to H_2O_2, fused to the KRAS C-terminal sequence or to RAB5 showed no PDGF-evoked change in fluorescence (Supplementary Fig. 8b). Furthermore, PDGF did not evoke significant ROS production at RAB5+ endosomes in TKO-MDFs (Supplementary Fig. 8c).

Collectively, these data strongly support a model in which PDGF-stimulation evokes formation of redoxosomes, recruiting and/or activating NOX complexes adjacent to the endocytosed PDGFR. Recruited NOX complexes catalyze ROS generation at these RAB5+ endosomes, resulting in spatially limited SHP2 oxidation. Alternatively,

SHP2-containing RAB5+/EEA1- vesicles could be recruited adjacent to, and possibly in contact with, NOX1/4-containing regions of the ER, resulting in exposure of RAB5+ vesicles/SHP2 to ER-localized ROS generation.

Redoxosomes prevent precocious PDGFRβ dephosphorylation

To assess the physiological role of PDGF-evoked redoxosome formation/SHP2 oxidation, we monitored the phosphorylation of PDGFRβ and its downstream signaling components in TKO-MDFs. PDGFRβ was degraded with similar kinetics following PDGF stimulation of WT- and TKO-MDFs (Supplementary Fig. 9a,b). In WT-MDFs, the relative tyrosyl phosphorylation of PDGFRβ peaked at around 10 min after stimulation, followed by a decay of phosphorylation at 30-120 min (Supplementary Fig. 9a,c). Compared with WT-MDFs, TKO-MDFs showed significantly decreased phosphorylation of Y579, Y716, Y857 and Y1009 in PDGFRβ at early times after ligand stimulation (1 min and 2.5 min), but comparable phosphorylation levels at later times (10 min and later; Fig. 6a and Supplementary Fig. 9a,c). These phosphorylation differences correlate temporally with ROS production at RAB5+ vesicles as detected by HyPer3 (Fig. 5b), ox-SHP2 generation (Fig. 3a), and ox-SHP2 localization near the PDGFRβ (Fig. 3b). Tyr-857 is an auto-phosphorylation site, which is necessary to enhance the kinase activity of PDGFRβ, whereas Y579, Y716 and Y1009 are reported binding sites for SHC/SRC/signal transducer and activator of transcription 5 (STAT5), growth factor receptor binding protein 2

(GRB2)/SOS and phospholipase Cγ (PLCγ)/SHP2, respectively[27]. Consistent with decreased phosphorylation of the latter PDGFRβ tyrosyl residues, phosphorylation of MEK1 (MAP kinase or ERK kinase-1) at S217 and S221 was decreased significantly in TKO-MDFs (Fig. 6b). Importantly, treatment with the allosteric SHP2 inhibitor SHP099[43] partially restored PDGFRβ tyrosine phosphorylation in TKO-MDFs, while having almost no effect on WT-MDFs (Fig. 6c). These data suggest that redoxosome generation spatially and temporally inhibits SHP2 and other PTPs to enable the proper level of PDGFR activation specifically at early times after ligand stimulation.

Notably, PDGF-dependent activation of ERK was suppressed by SHP099 in WT- and TKO-MDFs, regardless of PDGFRβ phosphorylation/activation (Fig. 6c). Hence, SHP2 has spatially distinct actions on negative regulation of the PDGFR, which appears only in the absence of NOX1/2/4, and on positive regulation in RAS/ERK pathway activation, respectively.

Discussion

Biochemical evidence has argued for an important role for growth factor-induced ROS production in cellular signaling[1] and for PTPs as critical ROS targets[6,7]. Yet with the exception of a conformation-specific scFv (single-chain variable fragment) that selectively detects the sulfenylamide form of PTP1B[21], there has been no way to visualize oxidized PTPs or other proteins within cells. We capitalized on the preferential reactivity of dimedone for the SOH form of oxidized protein-thiols[17,18], the availability of anti-dimedone-Cys antiserum[20] and the highly sensitive and specific PLA method[23] to visualize growth factor-evoked SHP2 oxidation.

Our experiments confirm that dimedone prefentially labels reversibly oxidized PTPs, most likely in the PTP-SOH state (Supplementary Fig. 1a-c). PTP-sulfenic acids convert to intramolecular sulfenylamides[8] or disulfides[44] *in vitro*, sulfenylamide state has been detected in cells by a PTP1B-SN-specific scFv[21]. However, the kinetics and stoichiometry of these conversions are unclear, due to our inability to monitor each of these forms in cells. Accordingly, these observations do not exclude the possibility of a pool of the PTP-SOH form in cells. Indeed, our *in vitro* dimedone-labeling experiments, combined with our dimedone-PLA results, strongly suggest that PTP-SOH species exist in cells.

Most importantly, our results show that SHP2 oxidation is regulated in space and time, and provide support for the "redoxosome" model[2]. We propose that

379 PDGF-dependent redoxosome formation and SHP2 oxidation occur as follows: 1) Upon
380 PDGF stimulation, PDGFR is activated, phosphorylated and recruits SHP2 and other
381 signaling molecules; 2) PDGFR is endocytosed in a clathrin/dynamin-dependent manner,
382 and recruits NOX1/4 at the endosomes; 3) PDGFR and NOX-containing vesicles, via a
383 PI3K activity-dependent process, produce $O_2^{\cdot -}$ in their interiors; 4) $O_2^{\cdot -}$ is either dismutated
384 inside the vesicle or diffuses to the cytoplasm to be dismutated, in either case generating a
385 localized H_2O_2 gradient; and 5) SHP2 bound to PDGFR and possibly other PTPs at/close to
386 the redoxosome are oxidized by localized H_2O_2, resulting in temporal inactivation of PTP
387 activity around PDGFR (Fig. 6d). Although PDGF evokes co-localization of PDGFRβ
388 and NOX proteins (Fig. 5a), how NOX1/4 is recruited to PDGFR containing endosome
389 remains to be elucidated. Conceivably, a small amount of plasma membrane-associated
390 NOXs are co-endocytosed with PDGFR to form redoxosomes. Alternatively, a fraction of
391 NOX proteins reside on cytoplasmic vesicular structures and these vesicles are recruited
392 and possibly fuse with PDGFR-containing endocytic vesicles. We also cannot exclude the
393 possibility that endocytosing vesicles are close enough to the ER or other structures where
394 NOXs reside and produce ROS.

395 The "redoxosomes" in IL-1 or TNFα signaling are reportedly RAB5+/EEA1+[2,45].
396 Redoxosome-produced ROS is required for TNF receptor-associated factor 6 (TRAF6)
397 recruitment to the endocytosed IL-1 receptor complex and for TRAF2 recruitment to the
398 TNF receptor complex, and consequently, for nuclear factor-κB (NF-κB) activation in

399 response to these ligands[2]. However, the critical target molecule(s) of ROS-evoked
400 oxidation for TNFα/IL-1 signal transduction has(ve) not been identified. Although
401 PDGF-stimulation also induces structures consistent with redoxosomes, these structures are
402 RAB5+/EEA1- (Fig. 3b,c). Whether RTK- and cytokine-evoked redoxosomes form in
403 distinct locations, or instead, these discrepancies reflect technical differences, requires
404 clarification. Notably, the earlier experiments could have enabled labeling of vesicles that
405 contain RAB5 and EEA1 even if ROS production had occurred only in the RAB5+/EEA1-
406 compartment[45]. Importantly, our assay enabled us to visualize a key signal relay molecule,
407 SHP2, undergoing physiological oxidation on, or in close proximity to, these structures,
408 providing direct evidence of spatially limited redoxosome-dependent protein oxidation.
409 Furthermore, our results suggest that redoxosome-mediated oxidation events are likely to
410 be common to a wide variety of receptor systems.

411 In the absence of ROS production at redoxosomes (i.e., in TKO-MDFs), failure to
412 inhibit SHP2 and/or other PTPs at endocytic vesicles diminishes PDGFR and MEK
413 activation in response to PDGF (Fig. 6). However, genetic and biochemical evidence
414 implicates SHP2, and in particular, its catalytic activity, as a positive (i.e., signal enhancing)
415 regulator of growth factor-dependent RAS/ERK activation[13,14]. Previous work also
416 indicates that SHP2 dephosphorylates the PDGFR[15]. Our observation that PDGFR-bound
417 SHP2 is oxidized/inactivated at early time-points, together with the requirement of SHP2
418 activity for ERK activation, indicates that these two roles for SHP2 are spatially segregated

and differentially regulated by ROS. Presumably, critical SHP2 substrates for RAS/ERK activation are accessed either before or after redoxosome action or at a distinct intracellular location. Recent data also suggest that SHP2 could have distinct functions proximal to, and distal from, EGFR activation[46].

Our results indicate NOX1/4-dependent SHP2 oxidation occurs in close proximity to specific endosomes in growth factor-stimulated fibroblasts. Previous reports showed that NOX2 is responsible for SHP2 oxidation in erythropoietin-stimulated endothelial progenitors[47] and that NOX4 is necessary for shear stress-evoked SHP2 oxidation in aortic endothelial cells[48], but those studies could not provide spatial information. These findings do, however, imply that different NOX(s) catalyze SHP2 oxidation in different cells or signaling contexts, perhaps dependent on differential NOX expression. Another report argued that p66SHC and mitochondria are critical for PDGF-evoked ROS production and oxidation of PTPs, including SHP2[37]. Although strong suppression of oxidized PTPs was observed in p66SHC-depleted cells when compared with normal cells, p66SHC-depleted cells still showed a PDGF-dependent increase of PTP oxidation in their experiments. Hence, PDGF might stimulate p66SHC/mitochondria-dependent and -independent ROS production.

Multiple PTPs are purported targets of ROS-catalyzed oxidation[1,6,7] and PTPs have multiple, and distinct, functions in cell signaling[3]. Restricting their oxidation spatially and temporally is likely to be of critical importance, and visualizing such events is of clear

interest. Yet with the exception of PTP1B oxidation in response to insulin stimulation[21], visualization of intracellular oxidation events has not been reported heretofore. Dimedome-PLA can also recognize insulin-evoked ox-PTP1B (Fig. 2), but because it capitalizes on the intrinsic chemistry of cysteine oxidation, our method is, in principle, adaptable to all PTP superfamily members, as well as any protein-thiols for which an appropriate antibody is available.

Methods

Cell Culture

Swiss 3T3 (3T3 Swiss albino) cells, *Ptpn11*$^{fl/fl}$ MEFs expressing CRE-ER^{Tam} (ref. 22), and HepG2 cells were cultured in Dulbecco-modified Eagle's medium (DMEM), supplemented with 10% fetal bovine serum (FBS). To induce deletion of *Ptpn11*, *Ptpn11*$^{fl/fl}$ MEFs were treated with 1 μM 4-hydroxytamoxifen (4OHT) for 4 days. Primary mouse dermal fibroblasts (MDFs)[41] were cultured in DMEM/F-12 supplemented with 10% FBS. Swiss 3T3 cells and HepG2 cells were from a Neel lab-maintained stock, and were authenticated by the CellCheck short tandem repeat (STR) profiling service (IDEXX BioResearch). All cells were tested for mycoplasma using the Mycoplasma Plus detection kit (Agilent).

Antibodies

Mouse monoclonal anti-SHP2 (B-1, sc-7384), anti-PDGFRβ–pY716 (F-10, sc-365464), anti-ERK2 (D-2, sc-1647), and anti-RAB5A antibody (E-11, sc-166600), as well as rabbit polyclonal anti-SHP2 (C-18, sc-280), anti-PDGFRβ (958, sc-432), anti-PDGFRβpY579 (sc-135671), and anti-calnexin (H-70, sc-11397), goat polyclonal anti-PDGFRβ (M-20, sc-1627), anti-clathrin heavy chain (C-20, sc-6579), anti-RAB5A (P-12, sc-26566), anti-EEA1 (C-15, sc-6414), anti-NOX1 (H-15, sc-5821), anti-NOX2 (C-15, sc-5827), anti-NOX3 (A-12, sc-34699), anti-NOX4 (N-15, sc-21860), and anti-p22phox (C-17, sc-11712) antibodies were purchased from Santa Cruz Biotechnology. Mouse monoclonal

466 anti-MEK1 (61B12, #2352) and anti-AKT1 (2H10, #2967), rabbit monoclonal
467 anti-PDGFRβpY857 (C43E9, #3170), anti-PDGFRβpY1009 (42F9, #3124) and anti-pAKT
468 T308 (244F9, #4056), as well as rabbit polyclonal anti-EEA1 (C45B10, #3288),
469 anti-pMEK S217/221 (#9121) and anti-pERK1/2 T202/Y204 (#9101) antibodies were
470 purchased from Cell Signaling. Mouse monoclonal anti-phosphotyrosine antibody cocktail
471 (4G10 platinum, 05-1050) and rabbit anti-dimedonylated cysteine antiserum (anti-cysteine
472 sulfenic acid, 07-2139) were purchased from Millipore. Mouse monoclonal anti-PTP1B
473 (ab201974) and chicken polyclonal anti-GFP (ab13970) antibodies were purchased from
474 Abcam. Goat polyclonal anti-PTP1B (AF3954) and anti-PDGFRβ (AF1042) antibodies
475 were purchased from R&D Systems. Mouse anti-FLAG antibody (M2, F1804) was
476 purchased from Sigma. Alexa fluor-conjugated secondary antibodies (Thermo Fisher) were
477 used for immunostaining. All antibodies were used at the concentrations recommended by
478 their manufacturers (1:1000 for immunoblotting and 1:500 for immunostaining), except for
479 anti-SHP2, anti-PTP1B antibodies and anti-dimedonylated cysteine antiserum for
480 dimedone-PLA (see below).
481
482 **Growth Factors and Chemical Compounds**
483 Recombinant human PDGF-BB and EGF were purchased from Peprotech.
484 5,5-Dimethyl-1,3-cyclohexanedione (dimedone), *para*-nitrophenyl phosphate (*p*NPP),
485 4-Hydroxytamoxifen (4OHT), *N*-acetyl-*L*-cysteine (NAC), *L*-buthionine-*S*,*R*-sulfoximine

(BSO), and diphenyleneiodonium (DPI) were purchased from Sigma. Catalase (*Aspergillus niger*) was purchased from Millipore. Dynasore[31] was kindly provided by Dr. T. Kirchhausen (Harvard Med. Sch.) or purchased from Sigma. Pitstop® 2[32] was purchased from Abcam. Imipramine-blue[38] was synthesized and kindly provided by Drs. N. Patel and H.W. Pauls (Campbell Family Institute for Breast Cancer Research, Princess Margaret Cancer Center, University Health Network, Toronto, Canada). MitoQ (Mitoquinone)[39] was purchased from BioTrend. SHP099[43] was purchased from Alputon Inc. Rhodamine phalloidin was purchased from Thermo Fisher Scientific.

Expression Constructs

Retroviral expression vectors for wild type SHP2 (WT SHP2) and C459E SHP2 ($SHP2^{C459E}$) were generated by subcloning human *PTPN11* cDNA into pMSCV-IRES-EGFP (Clontech). pSUPER-puro-based control shRNA or sh*PTPN1* retroviral expression vectors were designed to target 5'-CCGCCCAGAGGAGCTATATTC-3' or 5'-CCGCCCAAAGGAGTTACATTC-3', respectively, as reported[49]. Expression vectors for WT mPTP1B or $mPTP1B^{C215S}$ were generated by subcloning the appropriate cDNAs into the lentiviral expression vector pFB-neo. Expression vectors for EGFP-fused RAB5A, RAB7A, RAB9A, and RAB11A and pEGFP-WT Dynamin 2 and $Dynamin2^{K44A}$ were purchased from Addgene. A cDNA of mouse catalase which lacks its peroxisome-targeting sequence was purchased from

Addgene, and subcloned into pMSCV-IRES-EGFP, adding a start codon followed by a FLAG-tag encoding sequence at the 5' end. Expression vectors for HyPer3-tk, HyPer3-RAB5 and HyPer3-RAB7 were generated by fusing cDNAs for either the human KRAS C-terminal sequence, human *RABA5A* or *RAB7A* (Addgene) to the 3' end of *HyPer3* cDNA, respectively. All constructs were confirmed by DNA sequencing.

Transfection, Infection and Cell Sorting

Swiss 3T3 cells were transfected with the indicated expression vectors using Lipofectamine3000 (Thermo Fisher), according to the manufacturer's protocol. Twenty-four hours post-transfection, GFP-positive cells were isolated by FACS using a MoFlo (Beckman Coulter), and then were seeded for dimedone-PLA, immunostaining or immunoblotting. *Ptpn11*$^{fl/fl}$ MEFs expressing WT SHP2, or SHP2^{C459E}, and Swiss 3T3 cells expressing FLAG-catalase were generated by retroviral infection, according to the manufacturer's protocol (pMSCV retrovirus system, Clontech) followed by FACS for GFP-positive cells. HepG2 cells were infected stably with VSVG-pseudotyped retrovirus carrying control shRNA or sh*PTPN1*, and selected in puromycin. Cells were further infected with VSVG-pseudotyped retrovirus carrying expression vector for WT mPTP1B or mPTP1B^{C215S}, and selected in geneticin (G418).

***In Vitro* Phosphatase Assay and Dimedone-Labeling**

Purified recombinant human PTP1B (1-321) was kindly provided by Dr. N.K. Tonks (Cold Spring Harbor Laboratory, New York). PTP1B (0.5 μg ml^{-1}) was pre-incubated in a buffer containing 12.5 mM Hepes (pH 7.4), 0.25 mM EDTA and 35 μM DTT in the presence of 10 mM DTT, 80 μM H_2O_2, 320 μM H_2O_2 or 1 mM pervanadate for 30 min at room temperature (R.T.). To measure reversibility of oxidation, aliquots from these reactions were incubated further in the presence of 10 mM DTT and 5 U of catalase at R.T. for 3 h. Catalytic activity was then measured by using *p*NPP as substrate and pre-incubated PTP1B (125 ng) in 200 μl of phosphatase assay buffer (25 mM Hepes pH 7.4, 50 mM NaCl, 10 mM *p*NPP) for 5 min at 37°C. For *in vitro* dimedone-labeling, purified PTP1B (0.25 μg μl^{-1}) was incubated for 5 min at R.T. in the presence or absence of 5 mM dimedone in labeling buffer (12.5 mM Hepes, pH 7.4, 0.25 mM EDTA and 35 μM DTT) containing a final concentration of 10 mM DTT, 80 μM H_2O_2, 320 μM H_2O_2 or 1 mM pervanadate, as indicated. Two μl of each reaction were diluted into 148 μl of SDS-PAGE sample buffer, and subjected to SDS-PAGE, followed by immunoblotting with anti-dimedone-Cys and anti-PTP1B antibodies. For post-oxidation dimedone-labeling, purified PTP1B (0.5 μg μl^{-1}) was first incubated in labeling buffer with 10 mM DTT, 80 μM H_2O_2, or 320 μM H_2O_2 at R.T. for 30 min, and then further incubated for 5 min at R.T. after addition of an equal amount of 10 mM dimedone solution containing the same concentration of DTT or H_2O_2.

Dimedone-PLA

546 Swiss 3T3 (2 x 10^4) or HepG2 (5 x 10^4) cells were seeded on 12 mm, poly-*L*-lysine-coated
547 circular glass coverslips, and then were serum-starved for 16 h. After stimulation with the
548 indicated growth factor or H_2O_2, cells were rinsed with PBS and fixed with 4%
549 paraformaldehyde/PBS containing 5 mM dimedone/0.25% DMSO for 5 min at R.T. The
550 dimedone-containing fixation solution was prepared fresh before each experiment and
551 filtrated through a PES membrane with pore size=0.22 μm (Millipore). Cells were then
552 rinsed 6 times with PBS, permeabilized with 0.1% TritonX-100/0.2% BSA/PBS for 10 min,
553 and blocked in 1% BSA/PBS for 30 min. After incubation with primary antibodies
554 (anti-SHP2 antibody: 1:5,000 or anti-PTP1B: 1:2,000, with anti-dimedonylated cysteine
555 antiserum: 1:1,000) for 1 h at R.T., cells were subjected to PLA (Duolink In Situ Detection
556 Reagents Red, Sigma) with donkey anti-mouse (Duolink In Situ PLA Probe Anti-Mouse
557 MINUS, Sigma) or donkey anti-goat (Duolink In Situ PLA Probe Anti-Goat MINUS,
558 SIGMA) and anti-rabbit (Duolink In Situ PLA Probe Anti-Rabbit PLUS, SIGMA)
559 secondary antibodies, according to the manufacturer's protocol. After the PLA procedure,
560 cells were subjected to another round of sequential incubation with primary and Alexa
561 fluorophore-conjugated secondary antibodies for co-staining with markers or NOX proteins.
562 Coverslips were then mounted on glass slides using Prolongold containing DAPI (Thermo
563 Fisher). Images were obtained by using an LSM700 confocal microscopy system (Carl
564 Zeiss). Semi-super resolution microscopic images (AiryScan) were obtained by using an
565 LSM880 (Carl Zeiss).

566

567 **Immunofluorescence**

568 Cells (4 x 10^4 for anti-dimedone-Cys staining or 2 x 10^4 for other immunostaining) were
569 seeded on coverslips as above, fixed in 4% paraformaldehyde/PBS for 10 min at R.T.,
570 permeabilized with 0.1% TritonX-100, 0.2% BSA/PBS for 10 min, and blocked with 1%
571 BSA/PBS for 30 min, followed by sequential primary and secondary antibody treatments,
572 as indicated. Images were obtained by using an LSM700 or an LSM880.

573

574 **Immunoblotting**

575 Cells were lysed in SDS lysis buffer (50 mM Tris-HCl pH7.5, 100 mM NaCl, 1 mM EDTA,
576 1% SDS, 2 mM Na_3VO_4), and subjected to SDS-PAGE, followed by transfer to
577 Immobilon-FL PVDF membranes (Millipore). Membranes were blocked in 1% BSA/TBS
578 containing 0.1% Tween20 for 30 min, and treated with primary antibodies in blocking
579 buffer for 1 h, followed by treatment with IRDye-conjugated secondary antibodies
580 (LI-COR). Images were obtained by using an ODYSSEY CLx quantitative IR fluorescent
581 detection system (LI-COR), and quantified with Image Studio software Ver. 5.2 (LI-COR).

582

583 **Live-cell Imaging**

584 Expression vectors for HyPer3 or its mutants were transfected into Swiss 3T3 fibroblasts
585 using Lipofectamine 3000 (Thermo Fisher), as per the manufacturer's protocol. Twelve

hours after transfection, cells were re-seeded (1 x 10^4 cells/well) into glass-bottom 8-well lab-tech chambers (Nunc) or μ-Slide 8 Well (ibidi), and then serum-starved in phenol red-free DMEM for 16 h. The fluorescence intensities of HyPer3-expressing cells were monitored by using an LSM700 confocal microscopy system with a stage-top incubator at 37ºC in a 5% CO_2 atmosphere. Excitation was at 488 nm, and emission was monitored at 500-1000 nm. Images were obtained every 1 min, with PDGF added after the third scan. Cells that showed shrinking or detachment during the time-lapse were excluded from the analyses.

Image Analysis

For dimedone-PLA images, the number of punctate signals generated by PLA and nuclei were counted from a single image by using the "analyze particle" function of FIJI/ImageJ software[50]. HepG2 cell nuclei were counted manually. The number of PLA signals per cell was calculated by dividing the particle number by the number of nuclei in an image, averaging 6 images per condition. To assess the localization of ox-SHP2 within intracellular compartments, we employed object-based analysis, which enabled us to compare one signal representing many molecules (e.g., RAB5, EEA1, etc.) with another (PLA) representing a resolution-limited, sparse number of molecules. For object-based image analyses, regions of interest (ROIs) were set according to cell shape using FIJI/ImageJ software[50], and the region of the nucleus (stained with DAPI) was masked using CellProfiler software[51].

606 Punctate signals from PLA (red) and marker staining (green) were segmented by using Otsu
607 threshold algorithm in CellProfiler[51]. The centers of mass (CM) of the segmented objects
608 were determined by using MATLAB software (The MathWorks, Inc.). To evaluate potential
609 co-localization the nearest neighbor approach was applied by finding the distances between
610 the CMs of each red/green object to the nearest of the green objects in each cell. The
611 outliers in the obtained distances distributions were removed by using Tukey's method[52],
612 and the median distances of red-to-green and green-to-green in each cell (n = 50 cells per
613 condition) obtained using custom MATLAB scripts were subjected to statistical analyses.
614 For pixel-based co-localization analyses, 225 μm^2 (Fig. 5a) or 56.25 μm^2 (Supplementary
615 Fig. 8a) ROIs were set in cytoplasmic region of individual cells. Manders' and Pearson's
616 coefficients were calculated by setting the same threshold for ROIs for samples stained with
617 the same antibody, using the "coloc2" function in FIJI/ImageJ software[50]. For HyPer3
618 experiments, fluorescence intensities of each cell were obtained by setting a ROI according
619 to the cell shape, and subtracting background values. Relative fluorescence intensities were
620 calculated by setting the average intensity of the first 3 images (before PDGF stimulation)
621 to 1.
622
623 **Statistics and Reproducibility**
624 No statistical method was used to predetermine sample sizes. Samples were not randomized.
625 The investigators were not blinded to allocation during experiments or outcome assessment.

626 Sample sizes and statistical tests for each experiment are denoted in the figure legends.
627 Dimedone-PLA images shown in each panel represent one biological replicate. Each
628 dimedone-PLA experiment was performed at least twice (biological replicates), with
629 quantification of 6 fields of images (technical replicates), except Fig. 3d (15 cells), per
630 condition of the experiment. The absolute number of PLA puncta per cell in the same
631 culture condition varies between biological replicates, presumably because of subtle
632 differences in experimental conditions, but the fold-changes in number of PLA puncta
633 between the various conditions were reproducible. Therefore, each graph for PLA
634 quantification shows the result of one of the biological replicates. Each immunoblot was
635 performed four times (biological replicates) for quantification, or at least twice (biological
636 replicates) for expression checks. Each dimedone-PLA/marker co-staining experiment or
637 conventional immunostaining experiment was performed at least twice, and representative
638 images from one of the biological replicates are shown in each panel. Pixel-based image
639 analysis was performed with 10 (Fig. 5a) or 20 (Supplementary Fig. 8a) ROIs from 10 cells
640 per condition from one of the biological replicates, and object-based image analysis was
641 performed with 50 cells per condition. The results of live cell imaging are from independent
642 biological replicates. Statistical analysis was performed by using the two-tailed Welch's *t*
643 test (Figs. 1b, 5a, Supplementary Fig. 4c, 7c, 8a, 8c), unpaired/paired two-tailed *t* test (Fig.
644 6c, Supplementary Figs. 4c, 7c, 8a, 9c), or ANOVA with Bonferroni/Dunn's post-hoc test
645 (Figs. 1c, 2, 3b, 3d, 4a, 4b, 4c, Supplementary Figs. 1d, 1e, 1g, 2a, 2b, 2c, 2e, 3a, 5a, 6c,

646 6d) by using StatView software, where appropriate. Precise P values can be found in the
647 figures.
648
649 **Data Availability**
650 Source data for figures are available from the corresponding author upon request.
651
652 **Code Availability**
653 Computer codes for image analyses are available from the corresponding author upon
654 request.
655

References

1. Holmström, K. M. & Finkel T. Cellular mechanisms and physiological consequences of redox-dependent signalling. *Nat Rev. Mol. Cell. Biol*. **15**, 411-421 (2014).
2. Spencer, N. Y. & Engelhardt J. F. The basic biology of redoxosomes in cytokine-mediated signal transduction and implications for disease-specific therapies. *Biochemistry* **53**, 1551-1564 (2014).
3. Tonks, N. K. Protein tyrosine phosphatases: from genes, to function, to disease. *Nat. Rev. Mol. Cell. Biol.* **7**, 833-846 (2006).
4. Zhang, Z. Y. & Dixon, J. E. Protein tyrosine phosphatases: mechanism of catalysis and substrate specificity. *Adv. Enzymol. Relat. Areas Mol. Biol.* **68**, 1-36 (1994).
5. Peters, G. H., Frimurer, T. M. & Olsen, O. H. Electrostatic evaluation of the signature motif (H/V)CX5R(S/T) in protein-tyrosine phosphatases. *Biochemistry* **37**, 5383-5393 (1998).
6. Tonks, N. K. Redox redux: revisiting PTPs and the control of cell signaling. *Cell* **121**, 667-670 (2005).
7. Tanner, J. J., Parsons, Z. D., Cummings, A. H., Zhou, H. & Gates, K. S. Redox regulation of protein tyrosine phosphatases: structural and chemical aspects. *Antioxid. Redox Signal.* **15**, 77-97 (2011).
8. Salmeen, A. *et al.* Redox regulation of protein tyrosine phosphatase 1B involves a sulphenyl-amide intermediate. *Nature* **423**, 769-773 (2003).

9. Meng, T. C., Hsu, S. F. & Tonks, N. K. Development of a modified in-gel assay to identify protein tyrosine phosphatases that are oxidized and inactivated in vivo. *Methods* **35**, 28-36 (2005).

10. Boivin, B., Zhang, S., Arbiser, J. L., Zhang, Z. Y. & Tonks, N. K. A modified cysteinyl-labeling assay reveals reversible oxidation of protein tyrosine phosphatases in angiomyolipoma cells. *Proc. Natl. Acad. Sci. USA* **105**, 9959-9964 (2008).

11. Karisch, R. *et al*. Global proteomic assessment of the classical protein-tyrosine phosphatome and "Redoxome". *Cell* **146**, 826-840 (2011).

12. Paulsen, C. E. *et al*. Peroxide-dependent sulfenylation of the EGFR catalytic site enhances kinase activity. *Nat. Chem. Biol.* **11**, 57-64 (2011).

13. Chan, G., Kalaitzidis, D. & Neel, B. G. The tyrosine phosphatase Shp2 (PTPN11) in cancer. *Cancer Metastasis Rev.* **27**, 179-192 (2008).

14. Grossmann, K. S., Rosário, M., Birchmeier, C. & Birchmeier, W. The tyrosine phosphatase Shp2 in development and cancer. *Adv. Cancer Res.* **106**, 53-89 (2010).

15. Meng, T. C., Fukada, T. & Tonks, N. K. Reversible oxidation and inactivation of protein tyrosine phosphatases in vivo. *Mol. Cell* **9**, 387–399 (2002).

16. Kwon, J. *et al*. Receptor-stimulated oxidation of SHP-2 promotes T-cell adhesion through SLP-76-ADAP. *EMBO J.* **24**, 2331-2341 (2005).

17. Nelson, K. J. *et al*. Use of dimedone-based chemical probes for sulfenic acid detection methods to visualize and identify labeled proteins. *Methods Enzymol.* **473**, 95-115

(2010).

18. Poole, L. B., Zeng, B. B., Knaggs, S. A., Yakubu, M. & King, S. B. Synthesis of chemical probes to map sulfenic acid modifications on proteins. *Bioconjug Chem*. **16**, 1624-1628 (2005).

19. Huyer, G. *et al.* Mechanism of inhibition of protein-tyrosine phosphatases by vanadate and pervanadate. *J. Biol. Chem.* **272**, 843-851 (1997).

20. Seo, Y. H. & Carroll, K. S. Profiling protein thiol oxidation in tumor cells using sulfenic acid-specific antibodies. *Proc. Natl. Acad. Sci. USA* **106**, 16163-16168 (2009).

21. Haque, A., Andersen, J. N., Salmeen, A., Barford, D. & Tonks, N. K. Conformation-sensing antibodies stabilize the oxidized form of PTP1B and inhibit its phosphatase activity. *Cell* **147**, 185-198 (2011).

22. Yang, W. *et al*. An Shp2/SFK/Ras/Erk signaling pathway controls trophoblast stem cell survival. *Dev. Cell* **10**, 317-327 (2006).

23. Weibrecht, I. *et al.* Proximity ligation assays: a recent addition to the proteomics toolbox. *Expert Rev. Proteomics* **7**, 401-409 (2010).

24. Tsutsumi, R. *et al.* YAP and TAZ, Hippo signaling targets, act as a rheostat for nuclear SHP2 function. *Dev. Cell* **26**, 658-665 (2013).

25. Meng, T. C., Buckley, D. A., Galic, S., Tiganis, T. & Tonks, N. K. Regulation of insulin signaling through reversible oxidation of the protein-tyrosine phosphatases TC45 and PTP1B. *J. Biol. Chem.* **279**, 37716-37725 (2004).

716 26. Lemmon, M. A. & Schlessinger, J. Cell signaling by receptor tyrosine kinases. *Cell* **141,**
717 1117-1134 (2010).
718 27. Heldin, C. H. & Lennartsson, J. Structural and functional properties of platelet-derived
719 growth factor and stem cell factor receptors. *Cold Spring Harb. Perspect. Biol.* **5**,
720 a009100, doi: 10.1101/cshperspect.a009100 (2013).
721 28. Goh, L. K. & Sorkin, A. Endocytosis of receptor tyrosine kinases. *Cold Spring Harb.*
722 *Perspect. Biol.* **5**, a017459, doi: 10.1101/cshperspect.a017459 (2013).
723 29. Somsel Rodman, J. & Wandinger-Ness, A. Rab GTPases coordinate endocytosis. *J.*
724 *Cell Sci.* **13**, 183-192 (2000).
725 30. Simonsen, A. *et al*. EEA1 links PI(3)K function to Rab5 regulation of endosome fusion.
726 *Nature* **394**, 494-298 (1998).
727 31. Macia, E. *et al*. Dynasore, a cell-permeable inhibitor of dynamin. *Dev. Cell* **10**,
728 839-850 (2006).
729 32. von Kleist, L. *et al*. Role of the clathrin terminal domain in regulating coated pit
730 dynamics revealed by small molecule inhibition. *Cell* **146**, 471-484 (2011).
731 33. Damke, H., Baba, T., Warnock, D. E. & Schmid, S. L. Induction of mutant dynamin
732 specifically blocks endocytic coated vesicle formation. *J. Cell Biol.* **127**, 915-934
733 (1994).
734 34. Sundaresan, M., Yu, Z. X., Ferrans, V. J., Irani, K. & Finkel, T. Requirement for
735 generation of H_2O_2 for platelet-derived growth factor signal transduction. *Science* **270**,

296-299 (1995).

35. Sundaresan, M. *et al*. Regulation of reactive-oxygen-species generation in fibroblasts by Rac1. *Biochem J*. **318**, 379-382 (1996).

36. Bae, Y. S. *et al*. Platelet-derived growth factor-induced H_2O_2 production requires the activation of phosphatidylinositol 3-kinase. *J. Biol. Chem.* **275**, 10527-10531 (2000).

37. Frijhoff, J. *et al*. The mitochondrial reactive oxygen species regulator p66Shc controls PDGF-induced signaling and migration through protein tyrosine phosphatase oxidation. *Free Radic Biol Med* **68**, 268-277 (2014).

38. Munson, J. M. *et al*. Anti-invasive adjuvant therapy with imipramine blue enhances chemotherapeutic efficacy against glioma. *Sci. Transl. Med.* **4**, 127ra36, doi: 10.1126/scitranslmed.3003016 (2012).

39. Kelso, G. F. *et al*. Selective targeting of a redox-active ubiquinone to mitochondria within cells: antioxidant and antiapoptotic properties. *J. Biol. Chem.* **276**, 4588-4596 (2001).

40. Bedard, K. & Krause, K. H. The NOX family of ROS-generating NADPH oxidases: physiology and pathophysiology. *Physiol. Rev.* **87**, 245-313 (2007).

41. Rezende, F. *et al*. Unchanged NADPH Oxidase Activity in Nox1-Nox2-Nox4 Triple Knockout Mice: What Do NADPH-Stimulated Chemiluminescence Assays Really Detect? *Antioxid. Redox Signal.* doi:10.1089/ars.2015.6314 (2015).

42. Bilan, D. S. *et al*. HyPer-3: a genetically encoded H_2O_2 probe with improved

performance for ratiometric and fluorescence lifetime imaging. *ACS Chem. Biol.* **8**, 535-542 (2013).

43. Chen, Y. N. *et al*. Allosteric inhibition of SHP2 phosphatase inhibits cancers driven by receptor tyrosine kinases. *Nature* **535**, 148-152 (2016).

44. Chen, C. Y., Willard, D. & Rudolph, J. Redox regulation of SH2-domain-containing protein tyrosine phosphatases by two backdoor cysteines. *Biochemistry* **48**, 1399-1409 (2009)

45. Li, Q. *et al.* Nox2 and Rac1 regulate H_2O_2-dependent recruitment of TRAF6 to endosomal interleukin-1 receptor complexes. *Mol. Cell. Biol.* **26**, 140-154 (2006).

46. Furcht, C. M., Buonato, J. M. & Lazzara, M. J. EGFR-activated Src family kinases maintain GAB1-SHP2 complexes distal from EGFR. *Sci. Signal*. **8**, ra46, doi: 10.1126/scisignal.2005697 (2015).

47. Schröder, K. *et al.* NADPH oxidase Nox2 is required for hypoxia-induced mobilization of endothelial progenitor cells. *Circ Res.* **105**, 537-544 (2009).

48. Francisco, J. *et al.* NOX4-dependent Hydrogen peroxide promotes shear stress-induced SHP2 sulfenylation and eNOS activation. *Free Radic. Biol. Med.* **89**, 419-430 (2015).

49. Banh, R. S. *et al.* PTP1B controls non-mitochondrial oxygen consumption by regulating RNF213 to promote tumour survival during hypoxia. *Nat. Cell Biol.* **18**, 803-813 (2016).

50. Schindelin, J. *et al.* Fiji: an open-source platform for biological-image analysis. *Nature*

methods **9**, 676-682 (2012).

51. Kamentsky, L. *et al.* Improved structure, function, and compatibility for CellProfiler: modular high-throughput image analysis software. *Bioinformatics* **27**, 1179-1180 (2011)

52. Tukey, J. Exploratory Data Analysis. Addison-Wesley, 43-44 (1977).

ACKNOWLEDGEMENTS

We thank Drs. T. Kirchhausen (Harvard Medical School), N. Patel, H.W. Pauls (UHN Research, Toronto, Canada), and N.K. Tonks (Cold Spring Harbor Laboratory) for materials, Ms. X. Wang and Mr. R.S. Banh (Neel lab) for plasmids. We also thank Dr. J. Jonkman (UHN Research, Toronto, Canada) for technical instruction and Dr. M. Philips (NYU Medical Center) for helpful comments and discussion. This work was supported by NIH R37 CA49132 (to B.G.N.), and by grants from the Deutsche Forschungsgemeinschaft (DFG) SFB 974 (to P.I.H.B. and R.S.), SFB815/TP1 and SCHR1241/1-1 (to K.S.). B.G.N. was also a Canada Research Chair, Tier 1, and work in his Toronto lab was partially supported by the Princess Margaret Cancer Foundation. R.T. was supported by a Postdoctoral Fellowship for Research Abroad of the Japan Society for the Promotion of Science (JSPS).

AUTHOR CONTRIBUTIONS

R.T., P.I.H.B. and B.G.N. designed the research. R.T. performed experiments with the help of R.S. R.T. and J.H. analyzed the data. K.S. provided *Nox1,2,4*-triple KO MDFs. P.I.H.B. and R.S. provided HyPer3 expression vectors. R.T. and B.G.N. wrote the paper with advice from K.S. and P.I.H.B. B.G.N provided overall supervision for the research.

COMPETING FINANCIAL INTERESTS

803 The authors declare no competing financial interests.

804

805 **MATERIALS & CORRESPONDENCE.**

806 Correspondence should be addressed to Ryouhei Tsustumi (e-mail:

807 Ryohei.Tsustumi@nyumc.org)

808

809 **Figure Legends**

810 **Fig. 1.** Detection of oxidized SHP2 by dimedone-PLA. (**a**) Schematic illustrating method
811 for detecting oxidized SHP2 by dimedone-PLA. (**b**) Serum-starved Swiss 3T3 cells were
812 stimulated with PDGF-BB (50 ng ml^{-1}) for 10 min or left unstimulated. Cells were fixed in
813 the presence of dimedone (5 mM) for 5 min, and subjected to dimedone-PLA (red). Nuclei
814 were stained with DAPI (blue). Representative images are shown for each condition from
815 one of > 4 independent biological replicates. A higher magnification image of the boxed
816 region is shown at the bottom right. The graph shows the average number of PLA signals
817 per cell (n = 6 images for each condition, 5-20 cells in an image), relative to control cells
818 without stimulation (set as 1). The P value was calculated using a two-tailed Welch's t test.
819 Error bars represent SD. (**c**) Serum-starved *Ptpn11*$^{fl/fl}$ MEFs expressing CRE-ER^{Tam} treated
820 with or without 4-hydroxytamoxifen (4OHT) were stimulated with PDGF-BB (50 ng ml^{-1})
821 or H_2O_2 (1 mM) for 10 min. Cells were fixed in the presence of dimedone, and subjected to
822 dimedone-PLA (gray). Representative images are shown for each condition from one of 3
823 independent experiments. The graph shows average number of PLA signals per cell (n = 6
824 images for each condition, 5-20 cells in an image), relative to control cells without
825 stimulation (set as 1). ***P<0.0001, ANOVA with Bonferroni/Dunn's post-hoc test. Error
826 bars represent SD. Scale bars: 50 μm.
827

828 **Fig. 2.** Detection of oxidized PTP1B by dimedone-PLA. Serum-starved HepG2 cells
829 expressing control shRNA or shRNA targeting human *PTPN1* (sh*PTPN1*), with or without
830 stable expression of either mouse WT PTP1B or PTP1B^{C215S}, were stimulated with insulin
831 (25 nM) or H_2O_2 (1 mM) for 5 min or left unstimulated. Cells were then subjected to
832 dimedone-PLA with anti-dimedone-Cys and anti-mouse PTP1B antibodies (gray).
833 Representative images are shown for each condition from one of 2 independent biological
834 replicates. The graph shows the average number of PLA signals per cell (n = 6 images for
835 each condition, 80-120 cells in an image), relative to control cells without stimulation (set
836 as 1). ***P<0.0001, ns: not significant, ANOVA with Bonferroni/Dunn's post-hoc test.
837 Error bars represent SD. Scale bar: 50 μm.
838
839 **Fig. 3.** Spatio-temporal dynamics of SHP2 oxidation. (**a**) Serum-starved Swiss 3T3 cells
840 were stimulated with PDGF-BB (50 ng ml^{-1}) for the indicated times, and subjected to
841 dimedone-PLA. Representative images are shown for each condition from one of 2
842 independent experiments. The graph shows the average number of PLA signals per cell (n =
843 6 images for each condition, 5-20 cells in an image), relative to unstimulated control cells
844 (normalized to 1). Scale bar: 50 μm. (**b**) Serum-starved Swiss 3T3 cells were stimulated
845 with PDGF-BB (50 ng ml^{-1}) for the indicated times. Dimedone-PLA (magenta) and
846 co-staining with the indicated markers (green) are shown. Nuclei were stained with DAPI
847 (blue). Representative images are shown for each condition from one of 3 independent

848 experiments. Higher magnification images of the boxed regions are shown. Median
849 distances of centers of mass (CM) between punctate signals of ox-SHP2 and the nearest
850 indicated marker signal in cells were obtained by the object-based image analysis. The
851 box-whisker plots show the median inter-object distances at the indicated times after
852 stimulation (n = 50 cells, each time point). Boxes indicate the 25^{th}-75^{th} percentile; whiskers
853 represent the 5^{th}-95^{th} percentile. ***P<0.0001, ANOVA with Bonferroni/Dunn's post-hoc
854 test. Scale bar: 10 μm. (**c**) Serum-starved Swiss 3T3 cells were stimulated with PDGF-BB
855 (50 ng ml^{-1}) for 10 min, and subjected to dimedone-PLA (magenta) and co-staining with
856 indicated antibodies (green). Representative semi-super resolution microscopic images
857 (AiryScan) and higher magnification images of the boxed region from one of 2 independent
858 experiments are shown. Scale bars: 5 μm. (**d**) Swiss 3T3 cells expressing EGFP,
859 EGFP-fused wild type dynamin2 (WT Dynamin2) or dominant-negative dynamin2
860 (dynamin2^{K44A}) were serum-starved and stimulated with PDGF-BB (50 ng ml^{-1}) or H_2O_2 (1
861 mM) for 10 min, and subjected to dimedone-PLA. Representative images of co-staining of
862 dimedone-PLA (gray) and EGFP (green) are shown for each condition from one of 2
863 independent experiments. The graph represents the average number of PLA signals per cell
864 (n = 15 cells), relative to unstimulated control cells (normalized to 1). ***P<0.0001, ns: not
865 significant, ANOVA with Bonferroni/Dunn's post-hoc test. Scale bar: 50 μm. Error bars
866 represent SD.
867

868 **Fig. 4.** NOX complexes catalyze PDGF-evoked SHP2 oxidation. (**a**) Serum-starved Swiss
869 3T3 cells expressing EGFP or cytoplasmic catalase were stimulated with PDGF-BB (50 ng
870 ml^{-1}) or H_2O_2 (1 mM) for 10 min and subjected to dimedone-PLA (gray). Representative
871 images are shown for each condition from one of 2 independent experiments. (**b**)
872 Serum-starved Swiss 3T3 cells were left untreated or were pre-treated with DPI (2.5 μM)
873 (*top*) or imipramine-blue (6 μM) (*bottom*) for 5 min, stimulated with PDGF-BB (50 ng
874 ml^{-1}) or H_2O_2 (1 mM) for 10 min and subjected to dimedone-PLA (gray). Representative
875 images are shown for each condition from one of 2 independent experiments. (**c**)
876 Serum-starved primary murine dermal fibroblasts (MDFs) from wild type (WT) or *Nox1*,
877 *2,4* triple-KO (TKO) mice were stimulated with PDGF-BB (50 ng ml^{-1}) or H_2O_2 (1 mM)
878 for 10 min and subjected to dimedone-PLA (gray). Representative images are shown for
879 each condition from one of 3 independent experiments. (**a-c**) The graphs show the average
880 number of PLA signals per cell (n = 6 images for each condition, 5-15 cells in an image),
881 relative to control cells (normalized to 1). Error bars represent SD. ***P<0.0001, ns: not
882 significant, ANOVA with Bonferroni/Dunn's post-hoc test. Scale bar: 50 μm. (**d**)
883 Serum-starved Swiss 3T3 cells were stimulated with PDGF-BB (50 ng ml^{-1}) for 10 min,
884 and fixed in the presence of dimedone. Representative co-staining of ox-SHP2, detected by
885 dimedone-PLA (magenta), and the indicated NOX components (green) are shown from one
886 of 3 independent experiments (*top*). Nuclei were stained with DAPI (blue). Higher
887 magnification images of the boxed regions are shown. Scale bar: 10 μm. Median distances

888 of centers of mass (CM) between punctate signals of ox-SHP2 and the nearest indicated
889 NOX protein signal in cells were obtained by the object-based image analysis. Box-whisker
890 plots show median distances at 10 min after PDGF stimulation (*n* = 50 cells). Boxes
891 represent the 25^{th}-75^{th} percentiles and whiskers the 5^{th}-95^{th} percentiles.
892
893 **Fig. 5.** PDGF evokes redoxosome formation. (**a**) Serum-starved Swiss 3T3 cells were
894 stimulated with PDGF-BB (50 ng ml^{-1}) for 5 min, then immunostained with anti-PDGFRβ
895 (magenta) and the indicated anti-NOX component antibodies (green). Representative
896 images are shown for each condition from one of 2 independent experiments. Nuclei were
897 stained with DAPI (blue). Scale bar: 10 μm. The graph shows the average value of
898 Pearson's coefficient for PDGFRβ and indicated NOX components with or without
899 PDGF-BB stimulation (*n* = 1 ROI from each of 10 cells) ***$P<0.0001$; two-tailed Welch's *t*
900 test. (**b**) Serum-starved Swiss 3T3 cells expressing cytoplasmic HyPer3 (HyPer3-cyto),
901 plasma membrane-targeted HyPer3 (HyPer3-tk), RAB5-fused HyPer3 (HyPer3-RAB5) or
902 RAB7-fused HyPer3 (HyPer3-RAB7) were subjected to live-cell, time-lapse imaging. Top
903 panels: Fluorescence intensity (pseudo-colored) of each HyPer3 construct shown at one
904 minute intervals PDGF-BB (50 ng ml^{-1}) was added (arrow) after the third scan. Bottom
905 panel: Graph shows the means of the relative fluorescence intensities of individual cells (*n*
906 = 7 cells from each independent time-lapse experiment), setting the average of the first 3
907 time-points to 1 (*bottom*). Error bars represent SEM.

908

909 **Fig. 6.** NOX activity is necessary for PDGF signaling. (**a**) Serum-starved WT- or
910 TKO-MDFs were stimulated with PDGF-BB (50 ng ml^{-1}) for the indicated times. Lysates
911 were subjected to immunoblotting with the indicated antibodies. Representative
912 immunoblots are shown from one of 4 experiments. See also Supplementary Fig. 5a. Graph
913 at right shows percentage change in phosphorylation of the indicated PDGFRβ tyrosine
914 residues in WT- and TKO-MDFs at the indicated times post-stimulation, quantified from
915 immunoblots (n = 4). Error bars represent SD. (**b**) Serum-starved WT- or TKO-MDFs were
916 stimulated with PDGF-BB (50 ng ml^{-1}) for the indicated times. Lysates were subjected to
917 immunoblotting with anti-pMEK1/2 and anti-MEK1 antibodies. Representative
918 immunoblots are shown from one of 4 experiments. The graph shows the relative
919 phosphorylation of MEK1, quantified from the immunoblots (n = 4), with the value in
920 WT-MDFs at 5 min after PDGF stimulation set to 1. Data represent means ±SD. (**c**)
921 Serum-starved WT- or TKO-MDFs were pre-treated with SHP099 (5 μM) or vehicle for 30
922 min, and stimulated with PDGF-BB (50 ng ml^{-1}) for 2.5 min. Lysates were subjected to
923 immunoblotting with the indicated antibodies. Representative immunoblots are shown from
924 one of 4 experiments. The graph shows the relative phosphorylation of the indicated
925 PDGFRβ tyrosine residues, quantified from immunoblots (n = 4) with the values from
926 untreated WT- MDF set to 1. Data represent means ±SD. Values for each phosphotyrosine
927 residue in TKO-MDFs with or without SHP099 treatment were compared by paired

two-tailed *t* tests. (**d**) Schematic of PDGF-evoked redoxosome formation and SHP2 oxidation. See text for details.

Fig. 1

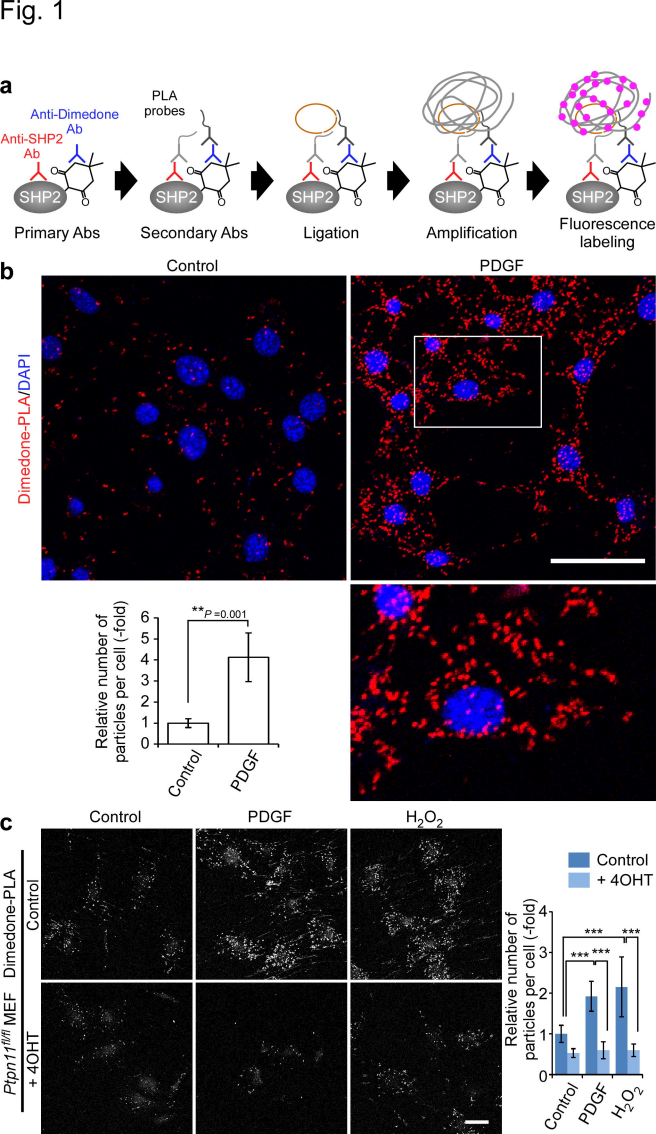
a
Anti-Dimedone Ab
Anti-SHP2 Ab
PLA probes
SHP2
Primary Abs
Secondary Abs
Ligation
Amplification
Fluorescence labeling
b
Control
PDGF
Dimedone-PLA/DAPI
Relative number of particles per cell (-fold)
**P =0.001
Control
PDGF
c
Control
PDGF
H2O2
Dimedone-PLA
Control
Ptpn11fl/fl MEF
+ 4OHT
Control
+ 4OHT
Relative number of particles per cell (-fold)
***
Control
PDGF
H2O2

Fig. 2

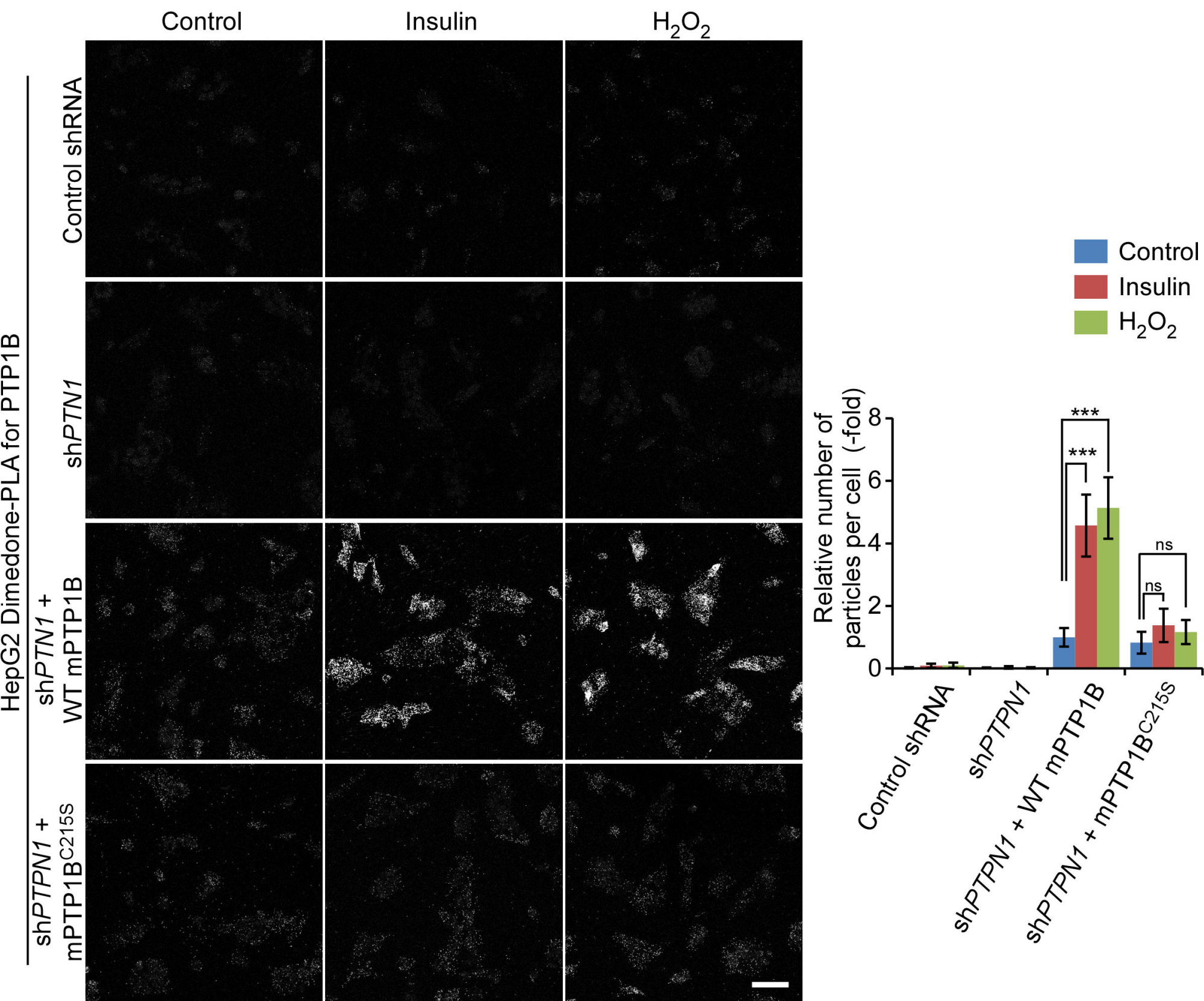
Control
Insulin
H_2O_2
HepG2 Dimedone-PLA for PTP1B
Control shRNA
sh*PTN1*
sh*PTN1* + WT mPTP1B
sh*PTN1* + mPTP1B^{C215S}
Control
Insulin
H_2O_2
Relative number of particles per cell (-fold)
0
2
4
6
8
***
***
ns
ns
Control shRNA
sh*PTPN1*
sh*PTPN1* + WT mPTP1B
sh*PTPN1* + mPTP1B^{C215S}

Fig. 3

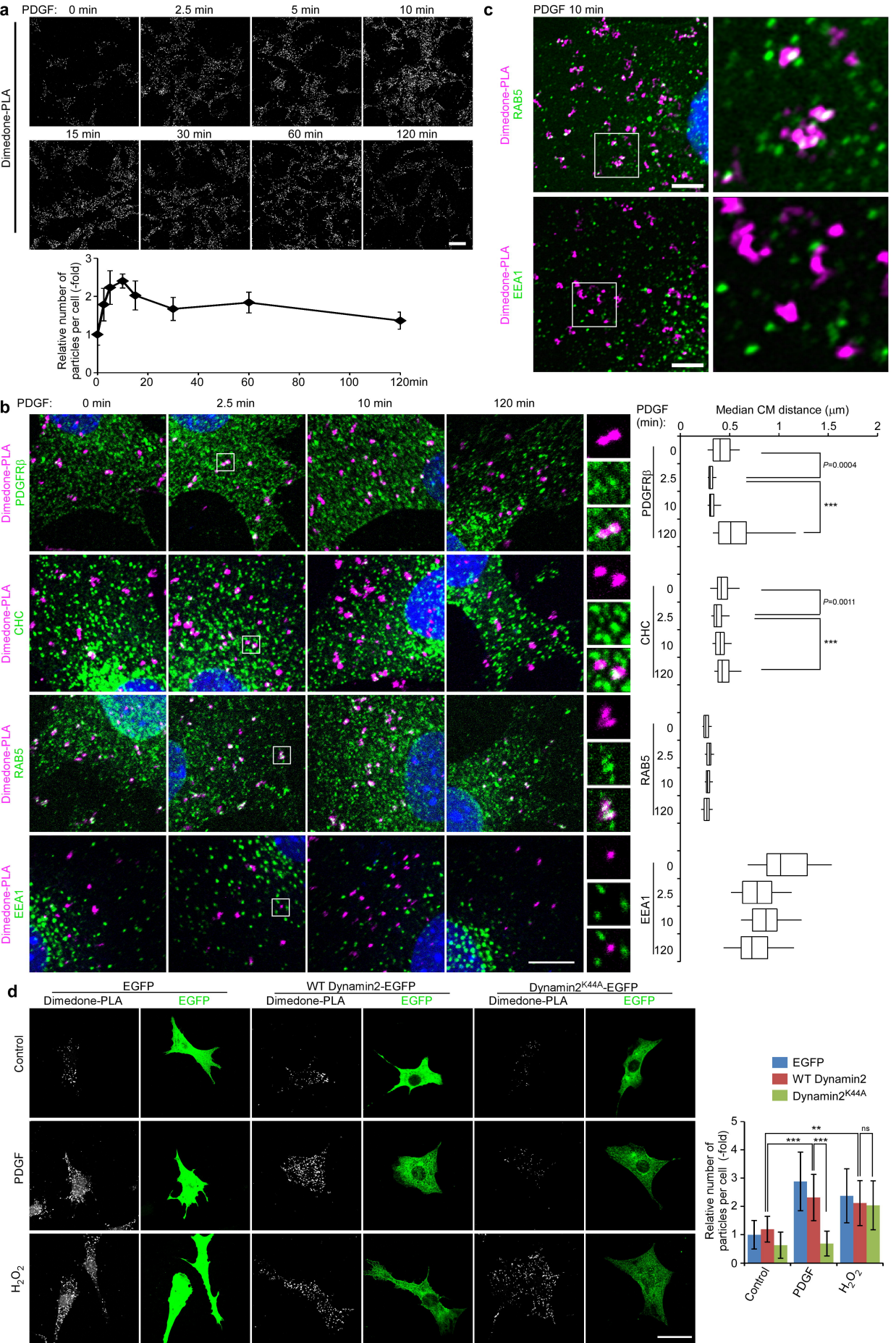
a
PDGF: 0 min
2.5 min
5 min
10 min
15 min
30 min
60 min
120 min
Dimedone-PLA
Relative number of particles per cell (-fold)
0
20
40
60
80
100
120min
c
PDGF 10 min
Dimedone-PLA RAB5
Dimedone-PLA EEA1
b
PDGF: 0 min
2.5 min
10 min
120 min
Dimedone-PLA PDGFRβ
Dimedone-PLA CHC
Dimedone-PLA RAB5
Dimedone-PLA EEA1
PDGF (min):
Median CM distance (μm)
0
0.5
1
1.5
2
PDGFRβ
CHC
RAB5
EEA1
P=0.0004
***
P=0.0011
***
d
EGFP
WT Dynamin2-EGFP
Dynamin2K44A-EGFP
Dimedone-PLA
EGFP
Control
PDGF
H2O2
EGFP
WT Dynamin2
Dynamin2K44A
Relative number of particles per cell (-fold)
**
ns
***
***
Control
PDGF
H2O2

Fig. 4

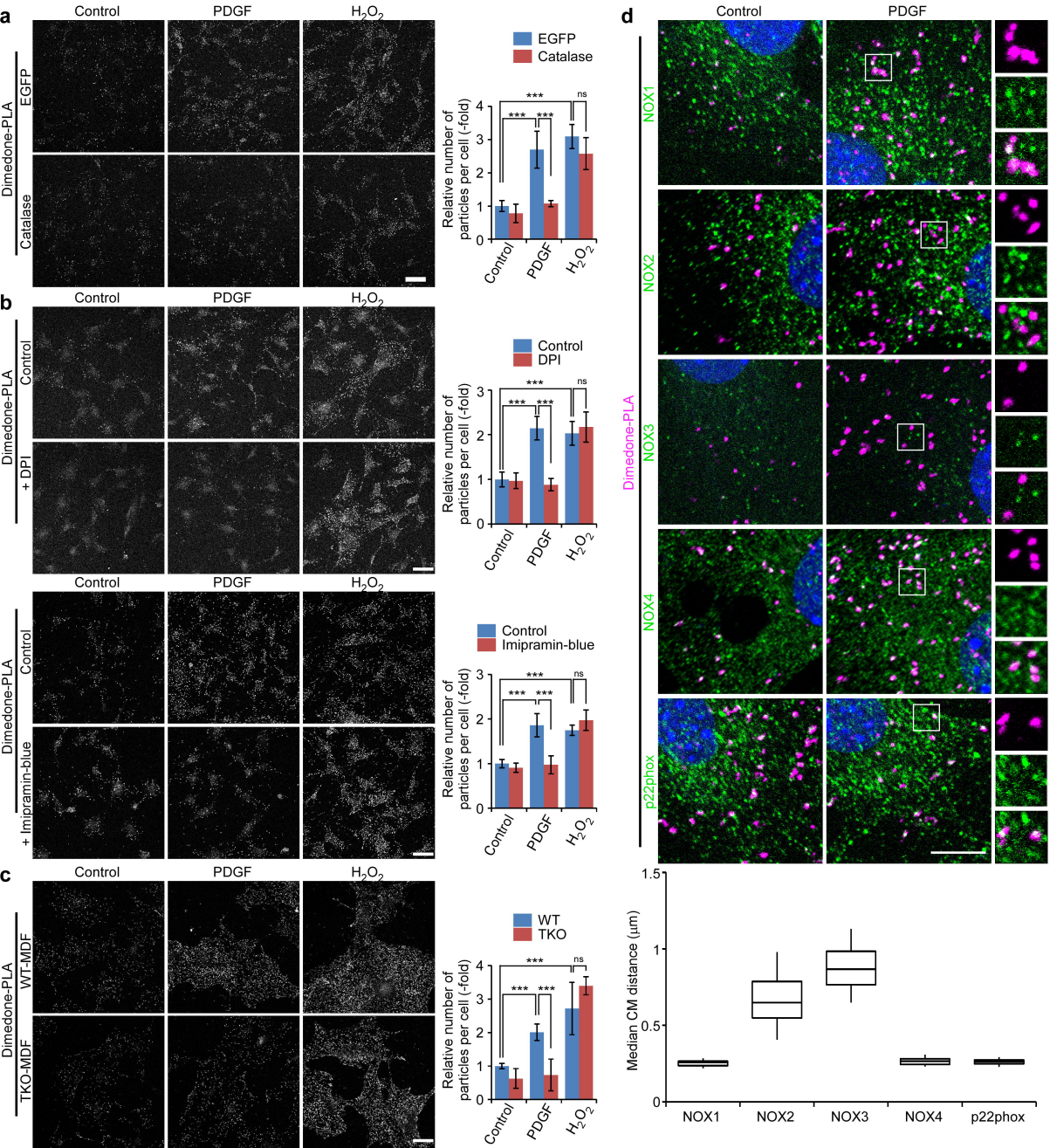
a
Control
PDGF
H_2O_2
Dimedone-PLA
EGFP
Catalase
EGFP
Catalase
Relative number of particles per cell (-fold)
***
ns
b
Control
DPI
+ DPI
c
WT
TKO
WT-MDF
TKO-MDF
Imipramin-blue
+ Imipramin-blue
d
NOX1
NOX2
NOX3
NOX4
p22phox
Median CM distance (µm)

Fig. 5

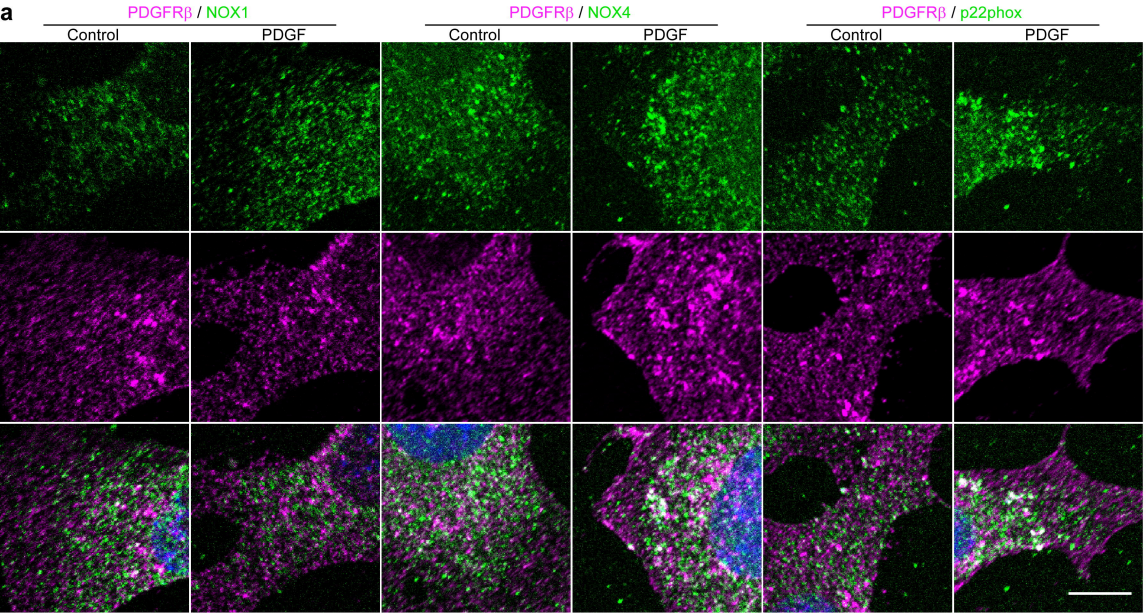
a
PDGFRβ / NOX1
Control
PDGF
PDGFRβ / NOX4
Control
PDGF
PDGFRβ / p22phox
Control
PDGF

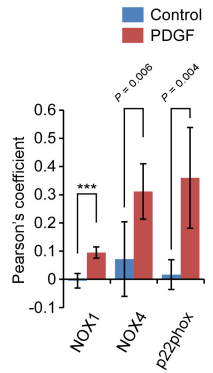
Control
PDGF
P = 0.006
P = 0.004
***
Pearson's coefficient
0.6
0.5
0.4
0.3
0.2
0.1
0
-0.1
NOX1
NOX4
p22phox

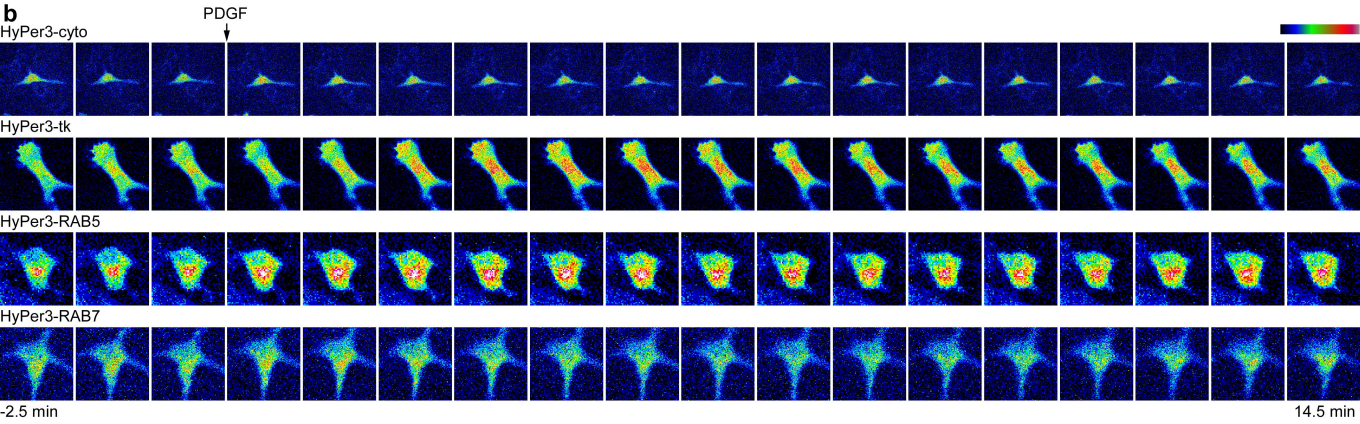
b
PDGF
HyPer3-cyto
HyPer3-tk
HyPer3-RAB5
HyPer3-RAB7
-2.5 min
14.5 min

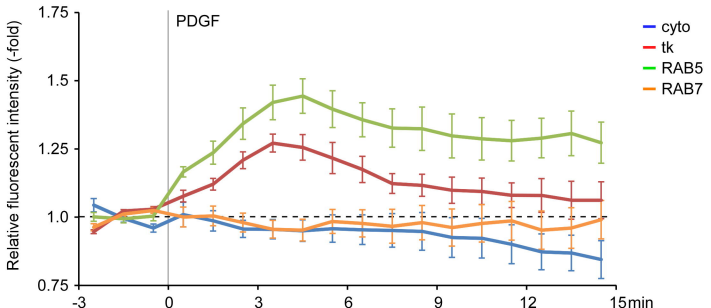
PDGF
Relative fluorescent intensity (-fold)
1.75
1.5
1.25
1.0
0.75
-3
0
3
6
9
12
15min
cyto
tk
RAB5
RAB7

Fig. 6

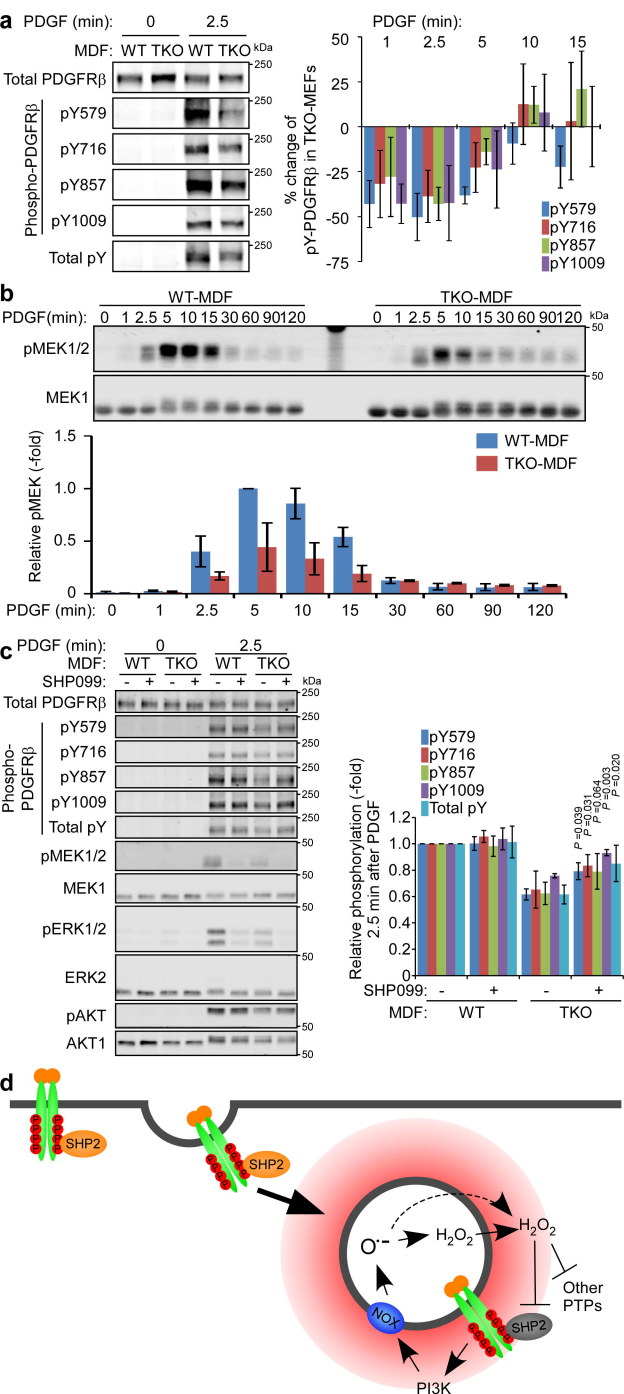
a
PDGF (min): 0 2.5
MDF: WT TKO WT TKO kDa
Total PDGFRβ
Phospho-PDGFRβ
pY579
pY716
pY857
pY1009
Total pY
250
PDGF (min): 1 2.5 5 10 15
% change of pY-PDGFRβ in TKO-MEFs
50 25 0 -25 -50 -75
pY579
pY716
pY857
pY1009
b
WT-MDF
TKO-MDF
PDGF(min): 0 1 2.5 5 10 15 30 60 90 120 0 1 2.5 5 10 15 30 60 90 120 kDa
pMEK1/2
MEK1
50
Relative pMEK (-fold)
1.5 1.0 0.5 0
WT-MDF
TKO-MDF
PDGF (min): 0 1 2.5 5 10 15 30 60 90 120
c
PDGF (min): 0 2.5
MDF: WT TKO WT TKO
SHP099: - + - + - + - + kDa
Total PDGFRβ
Phospho-PDGFRβ
pY579
pY716
pY857
pY1009
Total pY
pMEK1/2
MEK1
pERK1/2
ERK2
pAKT
AKT1
250
50
Relative phosphorylation (-fold) 2.5 min after PDGF
1.2 1.0 0.8 0.6 0.4 0.2 0
pY579
pY716
pY857
pY1009
Total pY
P=0.039
P=0.031
P=0.064
P=0.003
P=0.020
SHP099: - + - +
MDF: WT TKO
d
SHP2
SHP2
O2•-
H2O2
H2O2
Other PTPs
Nox
SHP2
PI3K